VTT Technical Research Centre of Finland

The importance of steel chemistry and thermal history on the sensitization behavior in austenitic stainless steels

Kolli, Satish; Javaheri, Vahid; Ohligschläger, Thomas; Kömi, Jukka; Porter, David

Published in:
Materials Today Communications

DOI:
10.1016/j.mtcomm.2020.101088

Published: 01/09/2020

Document Version
Publisher's final version

Materials Today Communications 24 (2020) 101088

Contents lists available at ScienceDirect

Materials Today Communications

journal homepage: www.elsevier.com/locate/mtcomm

The importance of steel chemistry and thermal history on the sensitization behavior in austenitic stainless steels: Experimental and modeling assessment

Satish Kolli[a,*], Vahid Javaheri[a], Thomas Ohligschläger[b], Jukka Kömi[a], David Porter[a]

[a] Materials and Mechanical Engineering, Centre for Advanced Steels Research, University of Oulu, 90014, Finland
[b] VTT Technical Research Centre of Finland, Finland

ARTICLE INFO

Keywords:
Stainless steels
Sensitization
Self-healing
CALPHAD
Thermo-Calc
Diffusion

ABSTRACT

The sensitization of austenitic stainless steels is dependent on various factors such as chemical composition, heat treatment temperature and time. To study these effects, the degree of sensitization in five austenitic stainless steel compositions that were subjected to isothermal heat treatments in the temperature range 550–820 °C has been determined using double loop electrochemical potentiokinetic reactivation testing. The nucleation and growth of grain boundary $M_{23}C_6$ carbides, that are responsible for sensitization, has been modelled with the help of the precipitation and diffusion modules in Thermo-Calc, assuming local multicomponent equilibrium, flux balance at the carbide-matrix interface, to quantitatively predict the Cr depletion. Based on the Cr depletion characteristics, a depletion parameter has been established that can predict sensitization in austenitic stainless steels and predict the effects of individual alloying elements.

1. Introduction

Austenitic stainless steels are prone to sensitization due to the formation of chromium carbides and corresponding Cr depleted zones. Bain et al. [1] was the first to observe that, during heat treatment of austenitic stainless steels in the temperature range 500 − 900 °C, chromium carbides precipitate along the grain boundaries. As the diffusivity of C is higher, C diffuses rapidly and all the C within an austenite grain is readily available for a growing grain boundary carbide, while Cr diffuses relatively slowly and is initially be drawn from the austenite adjacent to the carbide. This causes the Cr content of the austenite surrounding the carbides to initially drop below a level that is critical (12 % by wt.) with regard to corrosion resistance [2]. As the carbides are formed preferentially along the grain boundaries, this instigates intergranular corrosion. The depletion is controlled by two factors: one is the thermodynamics of the $M_{23}C_6$ formation and the other is the difference in the diffusivities of Cr and C. The formation of carbides occurs at temperatures where they are thermodynamically stable and where the diffusivity of Cr is sufficient for their nucleation and growth. The thermodynamics of carbide precipitation depends on the solubility of carbon at that particular temperature. This solubility of C depends on the bulk composition and these are precited using empirical relationships [3,4]. No Cr depletion below the critical level is observed at temperatures where the thermodynamics favors the formation of $M_{23}C_6$ carbide but the Cr diffusion is very rapid. Therefore, sensitization occurs in a relatively narrow temperature range.

Though sensitization depends on Cr depletion, previous studies show that the degree of sensitization measured from the electrochemical testing depends not only on the C and Cr concentrations but also on other variables including grain size [5–7], prior deformation [8] and the concentrations of other alloying elements [9,10]. Experimental quantification of sensitization and the understanding of the effects of different variables like time, temperature, grain size, strain, alloying elements on the magnitude of the sensitization has been widely studied [11–14].

The dependence of sensitization on the chemical composition of the material and particularly C content has been studied by many researchers. The predictions for the time required to develop sensitization using composition-based correlations were done by several researchers. The effective chromium content (Cr^{eff}) was calculated by giving proper weightage to each element according to its influence on the sensitization kinetics. This concept of effective chromium is originated by Cihal [15] and was well developed by Fullman [16]. With an increase in the bulk C content, the time required for sensitization decreases abruptly. Cihal proposed empirical relations involving elemental parameters to define effective Cr and C concentrations. In Fullman's work, this was

* Corresponding author.
E-mail address: satish.kolli@oulu.fi (S. Kolli).

https://doi.org/10.1016/j.mtcomm.2020.101088
Received 16 January 2020; Received in revised form 19 March 2020; Accepted 20 March 2020
Available online 23 March 2020

done by analyzing the thermodynamics of the precipitation of $M_{23}C_6$ carbides in the austenite matrix. He proposed effective chromium content Cr^{eff} parameter that includes the effects of major alloying elements on the Intergranular Stress Corrosion Cracking (IGSCC) susceptibility which agreed well with that of Cihal's parameters. Bruemmer studied the effect of composition with the help of a large database of temperature - time - sensitization (TTS) curves [17]. He predicted the time needed for sensitization to occur by modifying Cihal's elemental parameters to give the following *Composite Cr* concentration (Cr^*)

$$Cr^* = Cr + 1.6Mo - 0.2Ni - 100C \quad (1)$$

Parvathavarthini [18] explained sensitization kinetics in austenitic stainless steels by further modifying the *Composite Cr* to effective chromium content Cr^{eff}

$$Cr^{eff} = Cr + 1.45Mo - 0.19Ni - 100C + 0.13Mn - 0.22Si - 0.51Al - 0.20Co + 0.01Cu + 0.61Ti + 0.34V - 0.22W + 9.2N \quad (2)$$

In all of the above works, the compositional effects were established by empirical or semi-empirical relations. They did not involve the numerical prediction of the nucleation and growth of $M_{23}C_6$ carbides on the grain boundaries.

There are works on numerical prediction of Cr depletion profiles across the interface between $M_{23}C_6$ carbide and austenite matrix [19–23]. All of them either did not consider multicomponent diffusion or quantification with respect to experimentally measured sensitization values. Also, these works did not study the effect of composition variation on the Cr depletion characteristics and thereby sensitization. Following the approach used earlier by the author [24,25], the present work aims at predicting the effects of chemical composition on sensitization by simulating the nucleation and growth of $M_{23}C_6$ carbides and Cr depletion profile characteristics. The nucleation of carbides was simulated using TC-Prisma and growth using TC-DICTRA software which takes into account multicomponent diffusion effects.

2. Experiments and methodology

2.1. Materials

The investigated materials were 3 mm thick commercial 301 austenitic stainless steels provided by Outokumpu Stainless Oy, Tornio, Finland. Their chemical compositions are given in Table 1. The suffixes HiC, HiCr & LC indicate High carbon, High chromium and Low carbon alloys respectively.

The alloys vary from 6.72 to 15.89 values of Cr^{eff}, which represents low to higher sensitization resistance according to Bruemmer and Parvathavarthini [2,18] and is the motive to choose these alloys. All materials were homogenized by solution treatment at 1100 °C for 2 h followed by water quenching. To induce different degrees of sensitization, the homogenized material was then subjected to the heat treatments shown in Table 2.

2.2. Methods

All the sample conditions were subjected to double loop electrochemical potentiokinetic reactivation test testing to determine the degree of sensitization (DOS). The test has been performed according to the standard EN ISO 12732 [26]. The standard describes the limits of DOS values corresponding to highly sensitized, slightly sensitized and unsensitized material. The DOS obtained from this test is not sensitive to surface finish, hence samples were polished to a 600-grit surface finish. The test involves two polarization scans in opposite directions, where the forward anodic polarization scan causes the dissolution of all the surface irregularities and forms a passive film on the surface of the specimen. After establishing this passive film, the polarization scan in the reverse direction attacks the passive layer with dissolution occurring predominantly at chromium depleted regions that are susceptible to corrosion and this produces a reaction current peak [27]. This reactivation corrosion current density is a measure of the extent of Cr depletion at the grain boundaries [28]. The DOS value is the ratio of the reaction current density to the activation current density and is thus a measure of the ranges of sensitization in the material. The tests were conducted using VersaStat 3 potentiostat and standard solution 0.5 M H_2SO_4 + 0.01 M KSCN was used as the test medium. A scan rate of 6 V/h was used and the tests were performed at ambient temperature. Each of the tests was performed thrice. Both mean DOS and standard errors are recorded.

Table 1
Chemical compositions (wt.%) of all the alloy grades considered.

Steel grade	C	Cr	Ni	Si	N	Cr^{eff}
1.4310HiC	0.10	16.80	6.36	0.95	0.06	6.72
1.4301HiCr	0.05	18.10	9.07	0.44	0.03	12.35
1.4303HiCr	0.04	18.14	12.39	0.45	0.03	12.35
1.4307LC	0.02	18.12	8.08	0.37	0.05	15.40
1.4318LC	0.02	17.58	6.67	0.43	0.16	15.89

Table 2
Heat treatments to induce different levels of sensitization.

Steel grade	Heat treatment temperature (°C)	Holding time (h)
1.4310HiC	600, 650, 700, 760, 820	3,6,10,24,48,120,168
1.4301HiCr	600, 700, 820	3,10,24,48,120,168,240
1.4303HiCr	600, 700, 820	3,10,24,48,120,168,240,480
1.4307LC	550, 600, 700, 820	3,10,24,48,120,168,240,480
1.4318LC	550, 600, 700, 820	3,10,24,48,120,168,240,480

This test gives the degree of sensitization as a percentage which was normalized with respect to the smallest grain sized sample used in this study, i.e. 72 μm (1.4310HiC). Normalizing DOS this way compensates the effect of grain size on the reactivation peak current (I_r), through the length of the grain boundary [29]. Normalized degree of sensitization (NDOS) = $(I_r / I_a) \times (GS/72)$, where I_r is the maximum current for the reactivation loop (μA. cm^{-2}), I_a is the maximum current for the anodic loop (μA. cm^{-2}) and GS is the average grain size of the specimen (μm). The relative normalized values of DOS describe the depletion effects across the grain boundaries better, by compensating the effect of grain size on the total length of grain boundary in the tested specimen area.

A scanning transmission electron microscope (JOEL JEM-2200FS EFTEM/STEM) with an accelerating voltage of 200 kV was used in transmission and scanning transmission modes for the detailed observation of grain boundary precipitates and Cr concentrations. To prepare thin foils for the STEM studies, a FEI Helios Dual Beam Focussed Ion Beam (FIB) system was used with an accelerating voltage of 30 kV and beam currents in the range 90 pA to 9 nA. The FIB lamellae were then thinned and polished with an ion beam.

The precipitation module in Thermo-Calc, TC-Prisma [30], was used to estimate the nucleation times (τ) for the formation of $M_{23}C_6$ carbides. TC-Prisma implements the Kampmann-Wagner numerical method based on the Langer-Schwartz theory for the concurrent nucleation and growth of precipitate phases [31,32]. The interfacial energies, driving forces and the mobilities that are needed for the simulations are obtained from the thermodynamic and mobility databases TCFE7 and MOBFE2. The energy of the $M_{23}C_6$ - austenite interface is obtained as a function of temperature with the help of a modified Becker's model [31–33]. The calculated values were in the range $0.1 - 0.2\ J/m^2$, which are similar to others reported in the literature [34,35]. The molar volumes of phases were calculated on the basis of work by Qiu and Frisk [36,37].

The time dependent nucleation rate $J(t)$ is given by the extension of classical nucleation theory (CNT) for modeling nucleation in a multicomponent alloy system [38]. The incubation or nucleation time for an

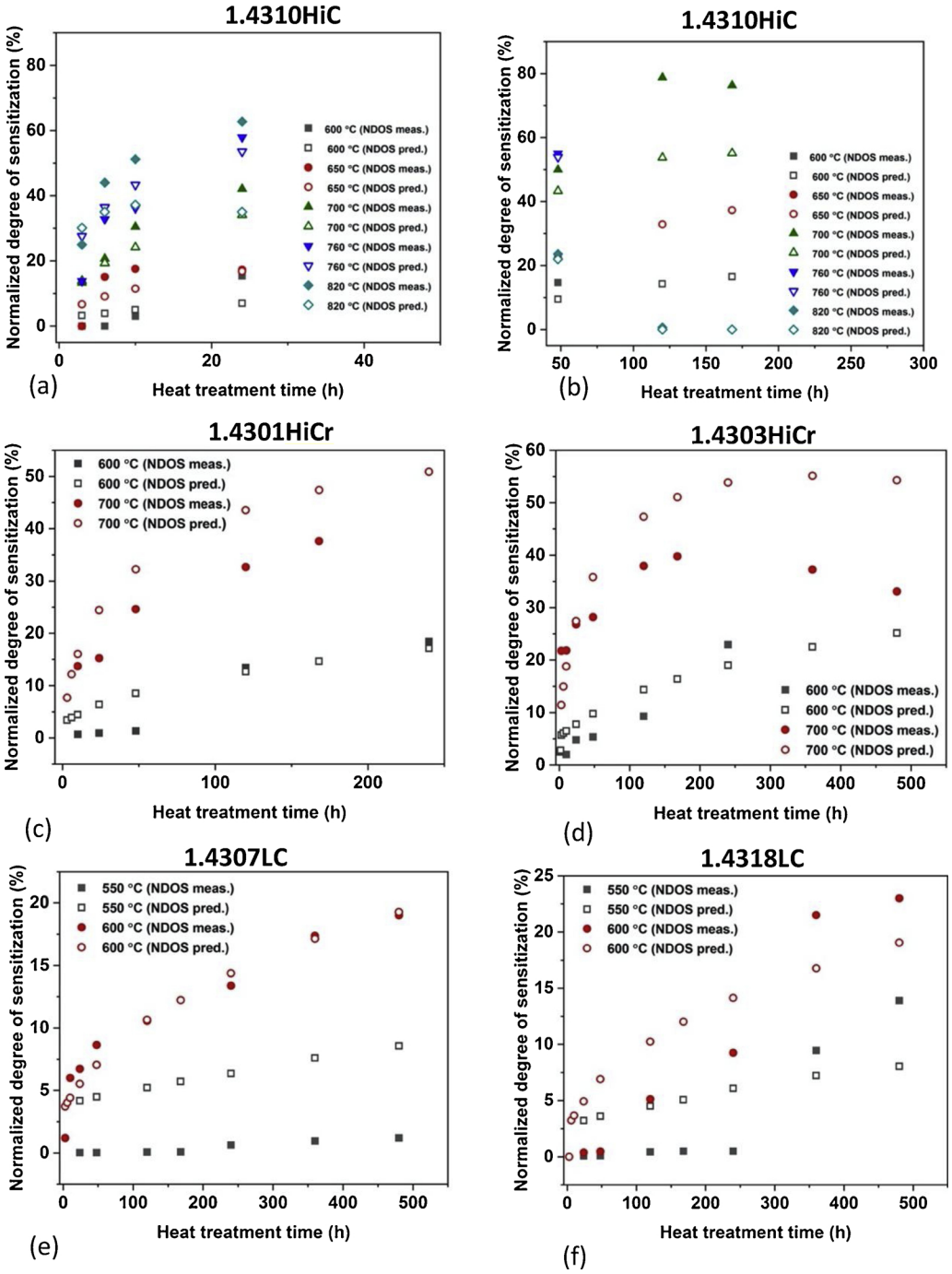

Fig. 1. NDOS values of all the sample conditions (measured from DL-EPR tests and predicted from the model discussed in later sections).

isothermal reaction is given by τ [39]

$$\tau = \frac{1}{2Z^2\beta^*} \tag{3}$$

Z is the Zeldovich factor, β^* is the rate at which atoms or molecules are attached to the critical nucleus,

$$\beta^* = \frac{4\pi r^{*2}}{a^4}\left[\sum_{i=1}^{k}\frac{\left(X_i^{\frac{\beta}{\alpha}} - X_i^{\frac{\alpha}{\beta}}\right)^2}{X_i^{\alpha/\beta}D_i}\right]^{-1} \tag{4}$$

a is the lattice parameter, $X_i^{\frac{\beta}{\alpha}}$ and $X_i^{\frac{\alpha}{\beta}}$ are the mole fractions of element i at the interface in the precipitate (β) and matrix (α) respectively, k denotes the number of components, D_i is the corresponding diffusion coefficient in the matrix, r* is the critical radius and is given by

$$r^* = -\frac{2\sigma V_m^{\beta}}{\Delta G_m^{\alpha\to\beta}} \tag{5}$$

σ is the interfacial energy, V_m is the molar volume of the matrix phase, ΔG^* is the Gibbs energy of formation of the critical nucleus,

$$\Delta G^* = \frac{16\pi\sigma^3}{3(\Delta G_m^{\alpha\to\beta}/V_m^{\beta})^2} \tag{6}$$

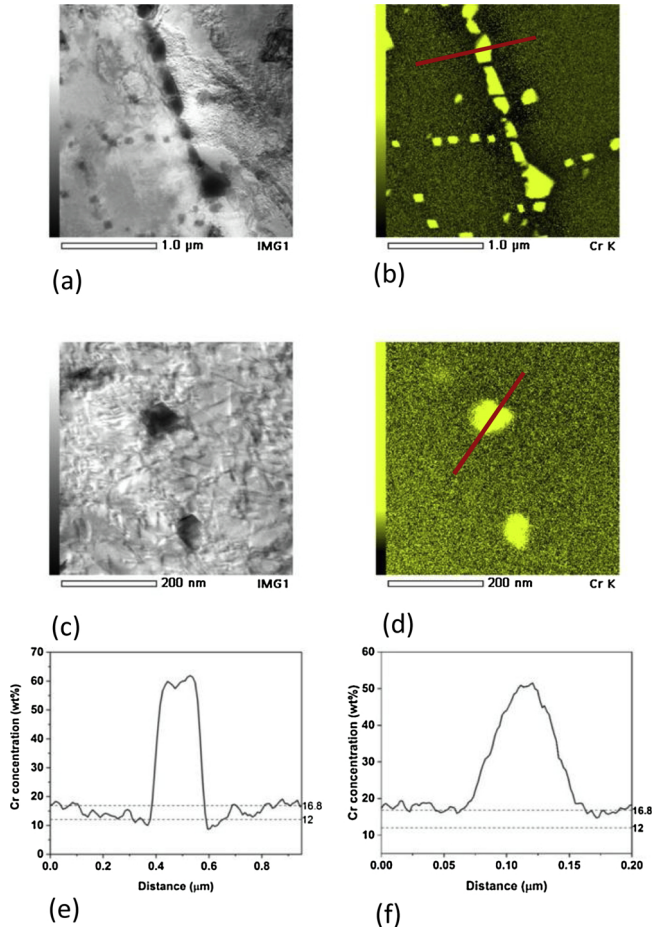

Fig. 2. (a, c) STEM micrographs (b, d) EDS mappings of Cr and (e, f) Cr concentration profiles along the red lines in (b, d) respectively for the sample condition 1.4310HiC −700 °C–120 h. (For interpretation of the references to colour in this figure legend, the reader is referred to the web version of this article).

The number of nucleating sites for the precipitation on grain boundaries is calculated from the density of grain boundary area [40]. The shape and size of the grains in the matrix control the number of nucleation sites available for precipitation. To calculate the available nucleation sites, it was assumed that all the grains are tetrakaidekahedra and that the grain boundary thickness is one atomic layer.

It was assumed that the growth of the $M_{23}C_6$ carbide starts after the nucleation time τ. The growth was simulated using the diffusion module in ThermoCalc, DICTRA [41]. The substitutional elements have much higher mobility along the grain boundaries than through the austenite matrix [42] and the grain boundaries are, therefore, expected to act as collector plates for the substitutional atoms delivering them to the grain boundary precipitates with a negligible concentration gradient in the grain boundary. Therefore, the diffusion and growth problem can be reduced to one dimension by assuming that the $M_{23}C_6$ covers the grain boundary and grows behind a planar austenite - carbide interface. The DICTRA simulations are based on a numerical solution of multicomponent diffusion equations that assume local equilibrium at the matrix-carbide interface [41]. As suggested by Sourmail [41] and also employed by Kolli et al. [25], the effect of soft-impingement is taken into account by considering the appropriate width of austenite from which carbon can be withdrawn as one sixth of the average grain size.

3. Experimental results

3.1. Degree of sensitization

The normalized degree of sensitization (NDOS) values for all the sample conditions obtained from DL-EPR test can be seen in Fig. 1. In the considered amount of time for heat treatments, NDOS is higher in 1.4310HiC compositions. Peak DOS was observed after 120 h of heat treatment at 700 °C in 1.4310HiC alloy. In both 1.4301HiC, 1.4303HiCr alloys, higher DOS and an equivalent amount of peak NDOS was observed at 700 °C. The observed NDOS values are lower in 1.4307LC and 1.4318LC, owing to their lower amount of carbon content. Sensitization and self-healing had been observed only in the case of 1.4310HiC at 820 °C. For the alloys 1.4307LC and 1.4318LC, no sensitization was observed at 700 °C even after 20 days of heat treatment. As Cr^{eff} suggests the effective Cr concentration in the steel, the higher the value of Cr^{eff}, the higher is the corrosion resistance in the alloy. From the Table 1, 1.4310HiC has least Cr^{eff} and thereby lower corrosion resistance that is evident from the DL-EPR tests results in Fig. 1. 1.4318LC has higher Cr^{eff}, and thereby higher corrosion resistance.

3.2. Precipitates and chromium depletion

Sensitized microstructures have already been well characterized [43,44]. The $M_{23}C_6$ precipitates responsible for sensitization mainly occurs on random high-angle grain boundaries with sizes and spacings that depend on the boundary in question. In this work, $M_{23}C_6$ carbides were identified in different sample conditions and the Cr concentration profiles (Cr depleted regions) across the $M_{23}C_6$ carbide - austenite matrix were measured using energy dispersive spectroscopy (EDS) in STEM.

Transmission electron microscopy studies were conducted on the samples that are sensitized and self-healed. Intergranular $M_{23}C_6$ carbides are observed and can be seen in the Figs. 2–4. In Fig. 2(a) STEM image of sample condition 1.4310HiC −700 °C −120 h is presented. Along with the grain boundary precipitates, precipitates are identified inside the grains (intragranular precipitates). Fig. 2(b) shows the EDS mapping of Cr for Fig. 2(a). The spot analysis on the precipitates reveal them to be $M_{23}C_6$ carbides. Fig. 2(c) shows the STEM image of intragranular $M_{23}C_6$ carbide and corresponding EDS mapping of Cr in Fig. 2(d). To observe the Cr concentration profiles across the carbide-matrix interface, line analysis has been done. The Cr concentration profiles shown by red lines in Fig. 2(b), (d) can be seen in Fig. 2(e), (f) respectively. Cr depletion has been detected in both the cases. In the case of grain boundary $M_{23}C_6$ carbide - austenite matrix interface, Cr fell below critical 12 % by wt. that is required for corrosion resistance. This supports DL-EPR measurements of NDOS (Fig. 1(a)) indicating the sample condition has been sensitized. In the case of intragranular $M_{23}C_6$-austentite matrix interface, the Cr is well above the critical level as evident from the Fig. 2(f).

The STEM image of the self-healed condition for the alloy 1.4310HiC is shown in Fig. 3(a) and the corresponding EDS mapping of Cr in Fig. 3(b). $M_{23}C_6$ carbides are noticed along the grain boundaries. The Cr concentration profile for the red line in Fig. 3(b) is plotted in Fig. 3(c). From the Cr depletion across the $M_{23}C_6$ - austenite matrix examinations it is clear that Cr did not go below the critical 12 % by wt. Cr. Thus, supporting the DL-EPR measurements, which insists the sample condition is completely self-healed.

Fig. 4(a), (c) show STEM images intergranular and intragranular $M_{23}C_6$ carbides in the sample condition 1.4303HiCr - 700 °C - 360 h, Fig. 4(b), (d) show the respective EDS mapping of Cr. Fig. 4(e), (f), show the Cr concentration profiles along the red lines in Fig. 4(b), (d). Similar to the observations in Figs. 2 and 3, Cr depletion was spotted and Cr fell below 12 % by wt. critical Cr content and did not go below critical 12 % by wt. across the intergranular and intragranular $M_{23}C_6$-austenite interfaces respectively. The sample condition was sensitized

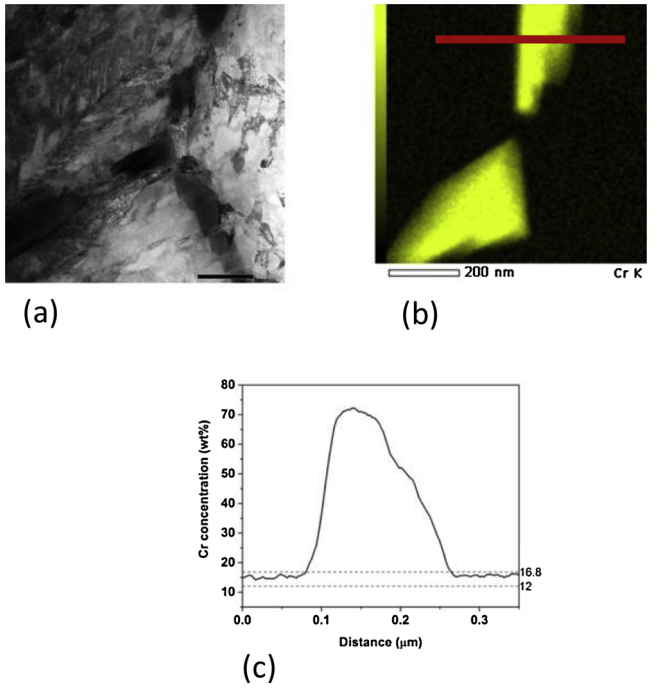

Fig. 3. (a) STEM micrograph (b) EDS mappings of Cr and (c) Cr concentration profiles along the red line in (b) for the sample condition 1.4310HiC −820 °C–120 h. (For interpretation of the references to colour in this figure legend, the reader is referred to the web version of this article).

according to DL-EPR measurements and was supported by the observed Cr concentration profile across grain boundary $M_{23}C_6$ - austenite matrix interface. Likewise, in 1.4303HiCr −700 °C −168 h, the Cr depletion below critical 12 % was observed only across the interface between grain boundary $M_{23}C_6$ - austenite matrix interface.

No sensitization was observed for the alloys 1.4307LC, 1.4318LC at 700 °C according to DL-EPR tests. In these sample conditions STEM measurements were made to verify the presence of $M_{23}C_6$ carbides and respective depletion zones. The $M_{23}C_6$ carbides and the corresponding Cr concentration profiles were observed. These indicate the presence of $M_{23}C_6$ carbides and the absence of Cr depleted zones below 12 % critical Cr.

3.3. Modelling the nucleation and growth of carbides

The nucleation times for all the heat-treated conditions calculated with TC-Prisma is given in Table 3. The nucleation times are higher at lower temperatures in all of the alloys. It can be seen that the nucleation time for grain boundary $M_{23}C_6$ carbides formation decreases with increase in temperature and are readily formed at 820 °C. The growth simulations are run after the nucleation times and the observed Cr concentration profiles across the grain boundary $M_{23}C_6$ - austenite matrix interface for chosen heat treatment conditions are shown in Fig. 5.

With increase in temperature, the chromium concentration in the austenite at the interface (Cr_{int}) increases. This is evident in all of the alloys in the Fig. 5. In the case of 1.4310HiC, for a heat treatment time of 120 h at 700 °C and 820 °C, the Cr_{int} increased from 6.49 to 12.62 wt. % Cr. W_{crit} is the effective width of chromium depleted zone at the grain boundary that is determined by the critical chromium concentration Cr_{crit} [45]. It was found that 12.5 Cr (wt.%) is the most appropriate value for considering as Cr_{crit} following Kolli et al. [25] as will be mentioned later. This W_{crit} initially increases with time at a given temperature and then decrease when the self-healing phase starts in the material.

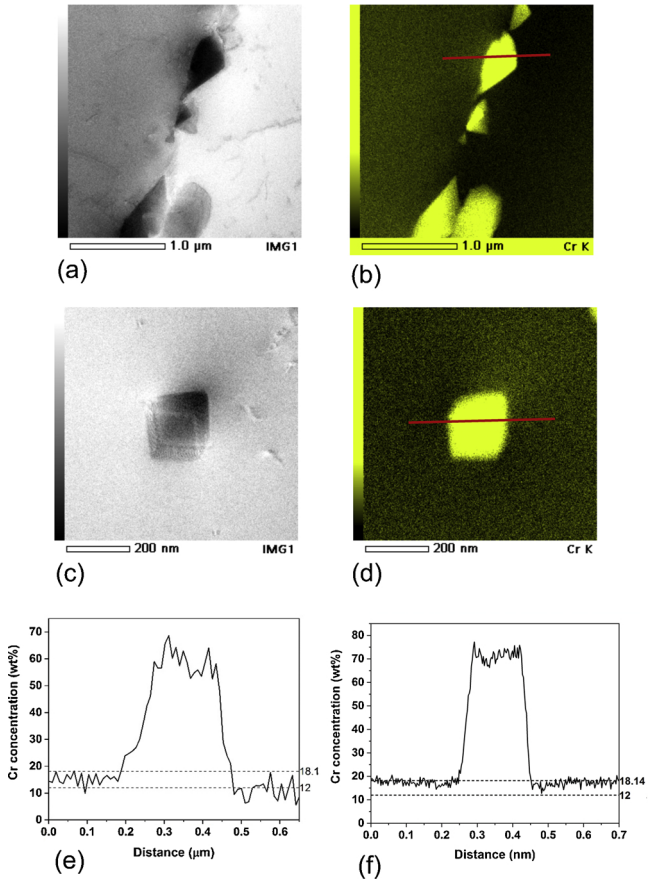

Fig. 4. (a, c) STEM micrographs (b, d) EDS mappings of Cr and (e, f) Cr concentration profiles along the red lines in (b, d) respectively for the sample condition 1.4303HiCr −700 °C–360 h. (For interpretation of the references to colour in this figure legend, the reader is referred to the web version of this article).

4. Discussion

In the sensitized microstructure, the chromium profiles are very narrow and it is challenging to measure them using STEM due to the possible inclination or curvature of the $M_{23}C_6$ - austenite matrix interface or the grain boundary. However, the microstructures that were sensitized have been well characterized [46,43]. The random high-angle grain boundaries are the favorable sites for the precipitation of $M_{23}C_6$ carbides. The size of the carbides varies from boundary to boundary. The $M_{23}C_6$ precipitates and the corresponding interface chromium concentration profiles in the severely sensitized sample condition 1.4310HiC −700 °C–120 h in Fig. 2 indicate the depletion of Cr below the critical 12 % and supporting the DL-EPR measurement. The same was observed in Fig. 4 for the sample condition 1.4303HiCr - 700 °C - 360 h. Fig. 3, 1.4310HiC −820 °C −120 h, shows the self-healed condition, where the Cr depletion did not below the critical level 12 % by wt. even in the presence of grain boundary $M_{23}C_6$ carbides due to the back diffusion of chromium from the bulk austenite to the interface with time.

To study the depletion characteristics, depletion parameter (DP) from the authors previous work [25] was used and it was defined as

$$DP = \begin{cases} (12.5 - \mathrm{Cr_{int}}) \bullet W_{crit}, & Cr_{int} > 10.0 \\ (12.5 - 10.0) \bullet W_{crit}, & Cr_{int} \leq 10.0 \end{cases} \quad (7)$$

where DP is measured in terms of nm.wt% i.e. using W_{crit} values

Table 3
Calculated nucleation times in seconds for the formation of grain boundary $M_{23}C_6$.

Alloy	% C (wt.)	Nucleation time (s)			
		550 °C	600 °C	700 °C	820 °C
1.4310HiC	0.10	–	4690	152	10
1.4301HiCr	0.04	–	4825	195	26
1.4303HiCr	0.04	–	3933	161	21
1.4307LC	0.02	58,833	8418	556	0
1.4318LC	0.02	85,108	13,032	1305	0

defined by Cr_{crit} = 12.5 wt.% and considering the minimum Cr_{int} to be 10 wt.%. This corresponds to the assumption that Cr contents below 10 wt.% in the depleted zone have no extra effect on the tendency to intergranular corrosion and DOS values. The observed statistical correlations between measured NDOS, calculated DP resulted in a very good fit with R^2 value of 0.90 and can be seen in Fig. 6. The predicted NDOS can be given by

$$NDOS_{predicted} = (0.21 \times DP) - (0.0002 \times DP^2) \quad (8)$$

where *DP* has the units (wt.%.nm). This inclusion of term bulk Cr, Cr^*, Cr^{eff} in the model to predict NDOS did not help in increasing the correlation for the fact that multicomponent diffusion has been considered in the modeling. The Eq. 8 suggests the increase in NDOS prediction with simultaneous increase in DP to some degree, and then saturates with further rise in DP. The predicted NDOS values are plotted against measured NDOS values in Fig. 1. The model predictions are largely in agreement with the experimentally measured values. However, the model over-predicted the NDOS values at lower temperatures as can be

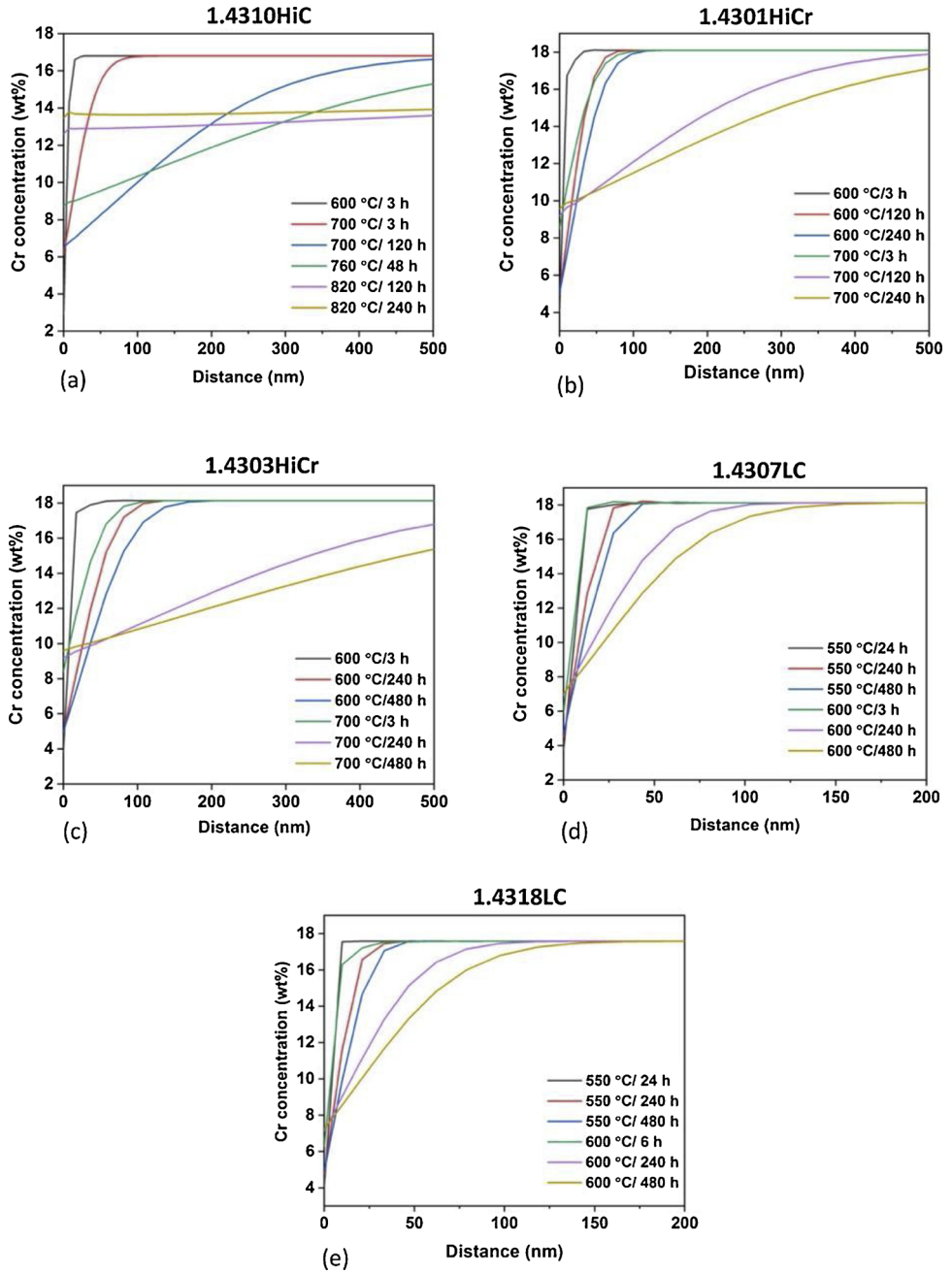

Fig. 5. Cr concentration profiles across the grain boundary carbide $M_{23}C_6$ - austenite matrix interface for all the alloy compositions considered for different isothermal heat treatment conditions.

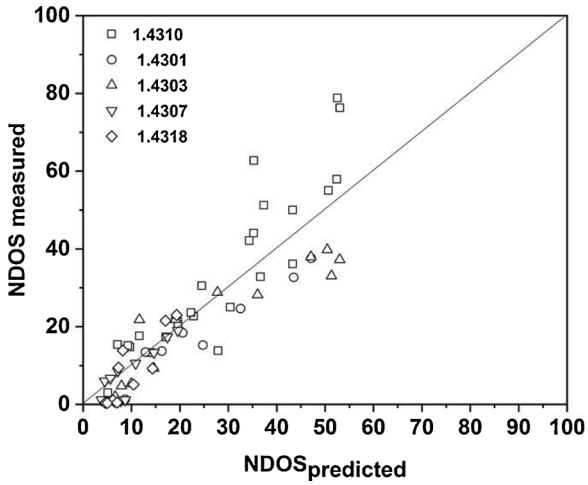

Fig. 6. Variation of measured NDOS and predicted NDOS (function of DP).

seen in Fig. 1(d, e) for 550 °C. The measured values of NDOS in these cases are very low, below 1 % NDOS and the very narrow chromium depletions predicted might not have any significant effect on the sensitization susceptibility.

4.1. Influence of chemical composition

Chromium and carbon are major compositional variables that control sensitization. However, other alloying elements can affect the sensitization kinetics too through their influence on the activities of carbon and chromium. Both the thermodynamics of $M_{23}C_6$ formation and the kinetics of chromium diffusion control the development of sensitized microstructure. The $M_{23}C_6$ carbides are generally thermodynamically stable below 900 °C and chromium diffusion is sufficiently rapid above 500 °C. The Time - Temperature - Precipitation (TTP) diagrams indicate the kinetics of $M_{23}C_6$ formation.

Fig. 7 shows Time - Temperature - Precipitation (TTP) diagrams for $M_{23}C_6$ on grain boundaries as calculated using the precipitation module in Thermo-Calc. The lines in the diagrams show the time to precipitate a volume fraction of 10^{-5}. Fig. 7(a) shows the TTP diagrams for all the steel grades considered in this work. The 'C' shape of the lines is due to the opposing effects of driving force for precipitation, which increases as the temperature decreases relative to the precipitate solvus, and the diffusion, which decreases with decreasing temperature. The decrease in carbon content from 1.4310HiC to 1.4318LC, shifts the TTP curve to longer times, contracts it into a narrower temperature range, and moves the nose of the curve to lower temperatures. Of course, elements other than carbon vary in the alloys studied. To explore the effect of carbon alone as well as the effects of the other alloying elements on the predicted precipitation kinetics, carbon, chromium and nickel were varied while keeping all other elements at their level in the alloy 1.4310HiC, see Fig. 7(b–d). As already indicated by Fig. 7(a), an increase in carbon raises the driving force for precipitation causing the TTP curves to shift to shorter times, raising the temperature at the nose of the curve, and increasing the range of temperatures over which precipitation of $M_{23}C_6$ can occur. The effect of carbon on the temperature range over which $M_{23}C_6$ can precipitate can be seen from the calculated phase diagrams in Fig. 8. Fig. 7(c) shows that an increase in chromium content results in the same trends as an increase in the carbon content as would be expected from the effects of carbon and chromium on the driving force for precipitation. The same was observed in Fig. 7(d) by changing the nickel in the alloy. Increasing the bulk nickel content decreases the solubility of carbon and thereby increases the driving force for the formation of $M_{23}C_6$ carbides. The same is shown in Fig. 8(c, d). The

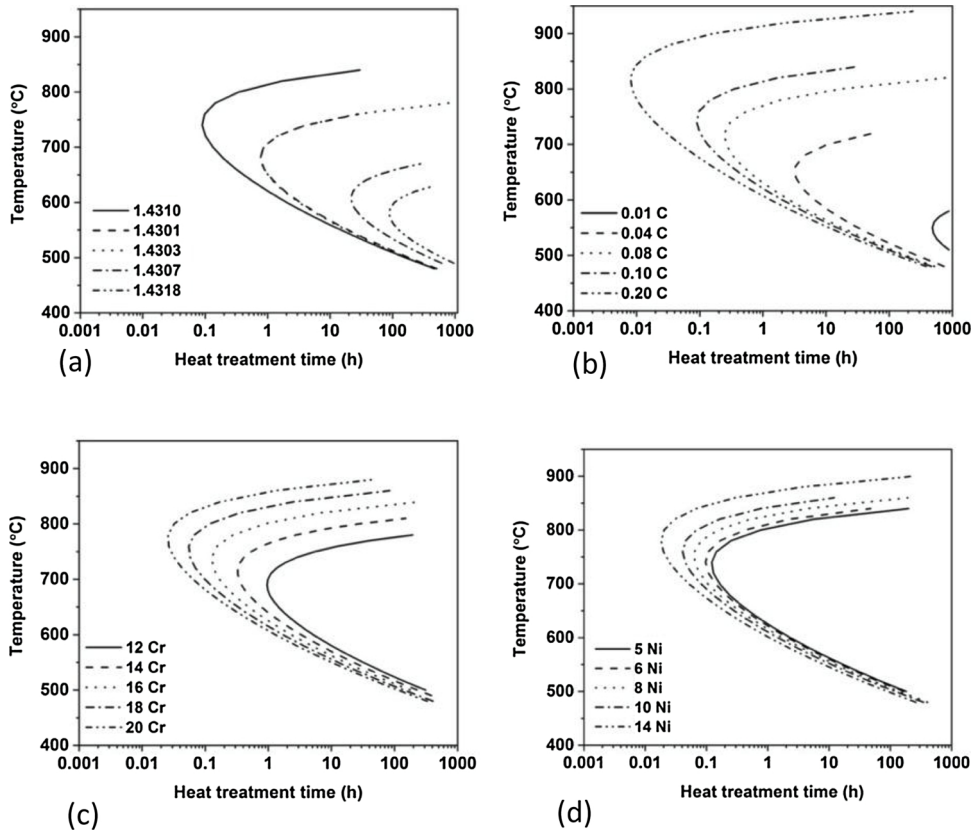

Fig. 7. Time - Temperature - Precipitation diagrams. (a) all the steel grades considered. The other diagrams show the effects of varying (b) C (c) Cr and (d) Ni when other elements are as they are in 1.4310HiC.

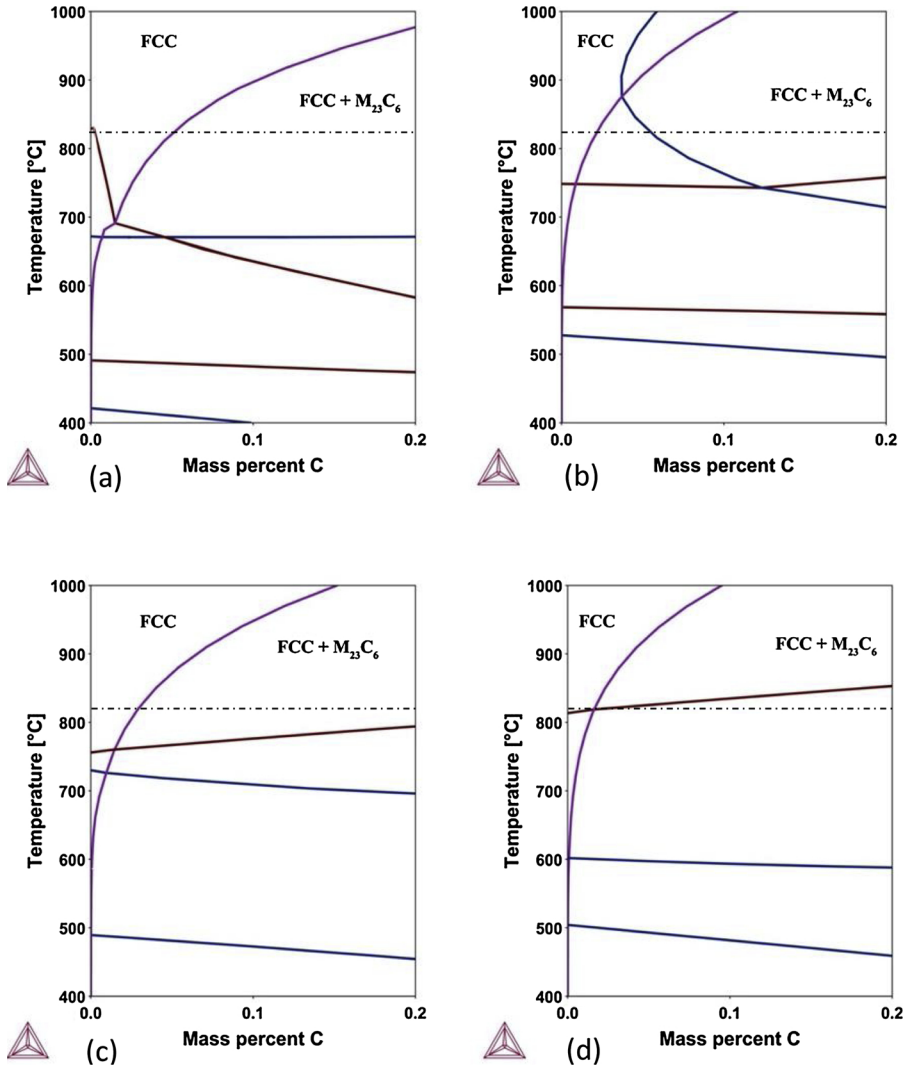

Fig. 8. Phase diagrams showing the effect of (a) chromium 12 % by wt. (b) 20 % by wt. and (c) nickel 4 % by wt. (d) 15 % by wt. on the solubility of carbon in austenite calculated from Thermo-Calc when other elements are as they are in 1.4310HiC alloy.

mobilities of carbon and nickel are also increased with increase in nickel content as is observed from the Thermo-Calc simulations. This resulted in shifting the TTP curve to shorter times and moving the nose to higher temperatures with an increase in nickel content. These TTP diagrams provide a preliminary information about the nucleation behavior and the trends with changing alloy compositions and thus signifying the importance of nucleation time in the modeling of the sensitization phenomenon.

4.2. Sensitization and self-healing kinetics

The model for predicting NDOS on the basis of the depletion parameter given earlier together with the precipitation and diffusion modules in Thermo-Calc can be used to predict the effects of individual alloying elements when all the other elements are kept constant. Fig. 9(a) shows the effect of carbon content on the sensitization and self-healing behavior at 820 °C. As can be seen, the time to reach the chromium depletion at the grain boundaries that causes 10 % NDOS decreases with an increase in carbon content. A low concentration of carbon in the austenite leads to slow $M_{23}C_6$ precipitation accompanied by less chromium depletion. In the 1D model considered, low carbon content means low carbon activity at the $M_{23}C_6$ - austenite interface and thereby high chromium activity. Also, a decrease in austenite carbon content decreases the mobility of chromium slightly, which plays a role in the sensitization caused by long annealing times, as is observed from the Thermo-Calc simulations. The peak NDOS is observed to increase when carbon content increases from 0.07 to 0.12 wt. % but remains unchanged with further increases up to 0.20 wt.%. The time to reach peak NDOS is predicted to increase up to 0.12 % C and thereafter decrease with further increases in carbon up to 0.20 %. The time to reach peak NDOS and thereby the chromium depletion at grain boundary $M_{23}C_6$- austenite matrix depends on the amount of $M_{23}C_6$ precipitation, which depends on the temperature and also the chromium diffusivity in the austenite matrix. Therefore, the trends in peak NDOS and the times to reach peak NDOS might be different at different temperatures than the 820 °C considered here. At a given temperature, precipitation kinetics are slower with lower carbon content (Fig. 9(b)). Lowering carbon content also decreases the diffusivity of chromium as is observed from the Thermo-Calc simulations. The trends in the times to reach peak NDOS are explained by the combined effects of the 'C´ type behavior of the TTP curve and the effect of carbon on chromium diffusivity. When the carbon content is less than 0.09, the formation of thermodynamically stable $M_{23}C_6$ is the controlling step. This formation of $M_{23}C_6$ becomes easier with increase in carbon content above 0.09 where chromium diffusivity becomes the limiting step.

The passivation characteristics of stainless steels are strongly affected by the chromium content, and the time to reach the chromium depletion at the grain boundaries that causes 10 % NDOS increases with

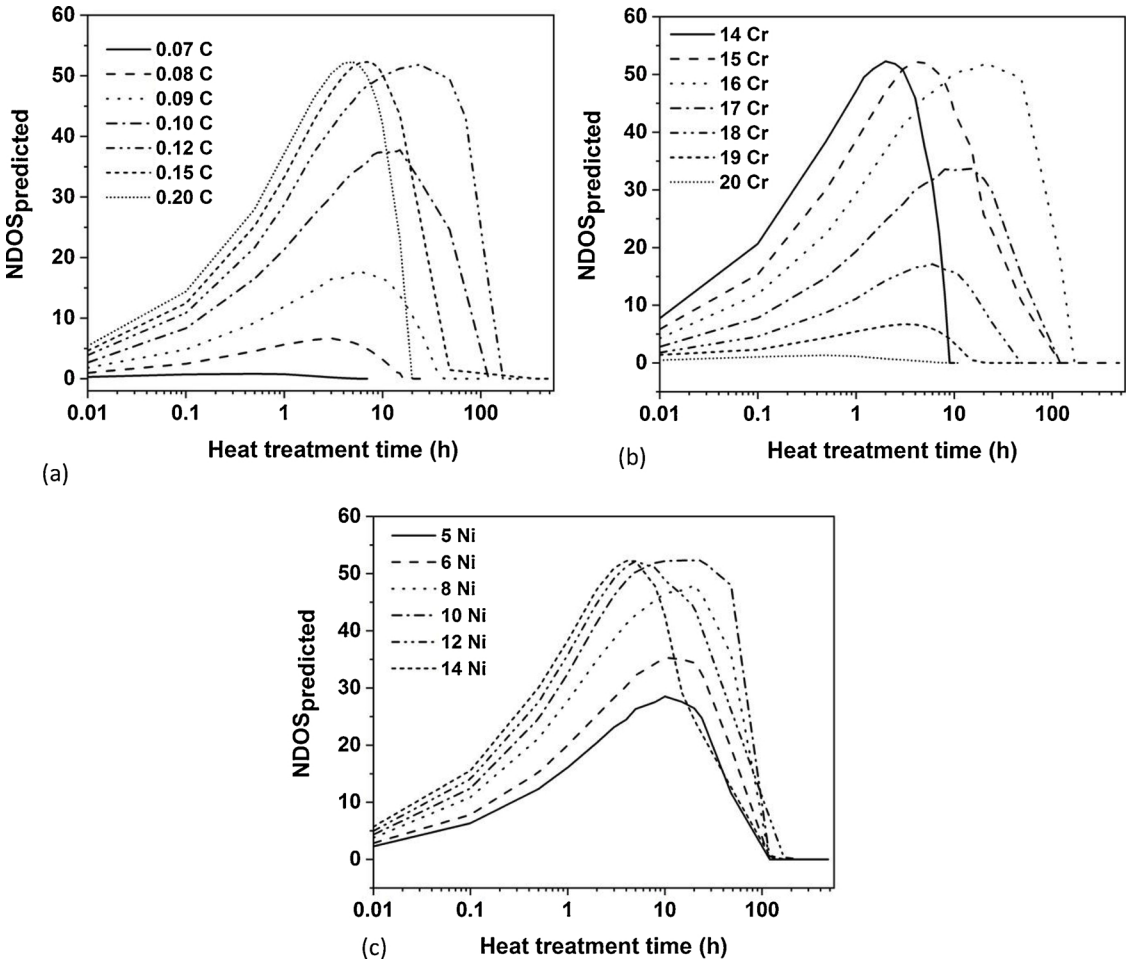

Fig. 9. NDOS predicted from the model extension with changes in (a) carbon, (b) chromium and (c) nickel and keeping all the other alloying elements constant and when the material is heat treated at 820 °C.

an increase in chromium content. These effects can be seen in the predicted influence of chromium content on the degree of sensitization shown in Fig. 9(b). Despite the fact that an increase in chromium accelerates the precipitation of $M_{23}C_6$ by raising the driving force for its precipitation, a higher level of chromium in the austenite hinders the depletion of chromium below the critical level of 12 % at grain boundary $M_{23}C_6$ - austenite matrix interface, even after relatively high degrees of precipitation. Lower chromium content gives lower chromium activity at the $M_{23}C_6$ - austenite interface, which results in combinations of Cr_{int} and W_{crit} that explain why NDOS values are predicted to decrease with an increase in the bulk chromium content. The peak NDOS was predicted to be constant for 14–16 % chromium thereafter declining up to 20 Cr. This is due to an increased back diffusion of chromium from the bulk into the depleted regions as chromium increases over the range 16–20 %. Back diffusion of chromium is less effective in the case of 14–16 % Cr leading to higher predicted peak NDOS values.

Nickel is an austenite stabilizer that needs to be increased to keep austenite stable as chromium increases. The effect of Ni on the TTP diagrams is visible from Fig. 7(d). Nickel decreases the solubility of carbon as can be seen from Fig. 8(c, d), thereby affecting the precipitation of $M_{23}C_6$ and thus shifting the TTP curve towards shorter times. An increase in Ni increases the mobility of chromium and carbon in austenite as observed from the simulations and thereby affects the depletion characteristics. An increase in nickel increases the NDOS at any given time during sensitization as can be seen from Fig. 9(c) and this can be attributed to the increased driving force for the formation of $M_{23}C_6$ carbides. From the depletion characteristics point of view, nickel increases the activity of carbon at the $M_{23}C_6$ carbide - austenite interface and thereby decreases the chromium activity resulting in lower Cr_{int} values and increased W_{crit} with time. The peak NDOS increases with increasing nickel content and can be related to the increased mobilities of chromium and carbon in the austenite along with the increased driving force for the formation of $M_{23}C_6$ carbides. The time to attain the peak NDOS, i.e. the start of self-healing, is predicted to be relatively insensitive to nickel content in the range 5–10 %, but shifting to shorter times from 10 to 14 % nickel. This shift is due to the increased mobility of chromium that results in the earlier appearance of the self-healing phase.

The relationship between NDOS and the proposed definition of the depletion parameter was obtained without considering any composition based empirical correlations like those that have been suggested earlier [17,18]. This has been possible by using the precipitation and diffusion modules in Thermo-Calc that take into account multicomponent effects in nucleation and diffusion to predict chromium concentration profiles away from grain boundaries. The approach used can thus be extended to obtain the sensitization behavior of any austenitic stainless steel and to critically understand the influence of each alloying element on the development of sensitization and self-healing. Using the model, NDOS as a function of temperature can be calculated which allows the generation of Time - Temperature - Sensitization (TTS) diagrams and cab be used as tools in the prediction of sensitization during isothermal heat treatments.

The current approach was used to explore the possible validity of using the effective chromium concentration Cr^* and Cr^{eff} as described in Eqs. 1 and 2 respectively to predict sensitization. However, using Eq. 8

to predict the time to reach 5 % NDOS in the alloys Fig. 9(b–d) showed that it was unattainable to obtain any correlation involving Cr^* and Cr^{eff}. The formula for Cr^{eff} is mainly based on a narrow range of compositions covered by 304 and 316 stainless steels and temperatures ranging from 600 to 700 °C. Nevertheless, when the range is extended to give Cr^{eff} values ranging from 5 to 18 and temperatures ranging from 500 to 820 °C, no correlation is predicted to exist. As shown above, the reason is that the phenomena controlling sensitization cannot be compressed into a simple composition parameter.

5. Conclusions

The sensitization and self-healing of 301 austenitic stainless steels having chemical compositions in the range 0.02 C, 16.80 Cr, 6.36 Ni to 0.10 C, 18.14 Cr, 12.39 Ni heat treated in the temperature range 550–820 °C has been studied experimentally with the help of DL-EPR testing. Results were normalized to compensate for variations in grain size between the various compositions. Transmission electron microscopy was used to identify the $M_{23}C_6$ carbides and the chromium concentrations at the $M_{23}C_6$ carbide - austenite matrix interface. It is shown that a chromium depletion parameter based on chromium concentration profiles calculated using Thermo-Calc DICTRA and Prisma software can be used to rather successfully predict both sensitization and self-healing kinetics. Deviations of predicted from experimental values can be attributed to the appearance of *intragranular* $M_{23}C_6$ carbides that were not accounted for in the one-dimensional DICTRA model. Applying the model to study the effects of individual alloying elements indicated that an increase in carbon and nickel contents increases the sensitization kinetics owing to an increased driving force for grain boundary carbide precipitation and an increase in the activity of carbon at the carbide - matrix interface. The model also predicted that sensitization kinetics become slower when the chromium content exceeds 16 wt.% as a result of increased chromium activity at the interface and increased chromium mobility in the austenite matrix.

Declaration of Competing Interest

The authors declare that they have no known competing financial interests or personal relationships that could have appeared to influence the work reported in this paper.

Acknowledgements

The authors would like to thank Tornio R&D Center, Outokumpu for providing the material for the study. The authors are grateful for the this project that has received funding from the European Union's Horizon 2020 research and innovation programme under the Marie Skłodowska-Curie grant agreement No 675715.

References

[1] E.C. Bain, R. Aborn, J. Rutherford, The nature and prevention of intergranular corrosion in austenitic stainless steels, Trans. Am. Soc. Steel Treat. 21 (1933) 481–509.
[2] S.M. Bruemmer, Quantitative measurement and modeling of sensitization development in stainless steels, Corrosion 46 (1990) 556–562, https://doi.org/10.6083/M44J0C21.
[3] M. Deighton, Solubility of $M_{23}C_6$ in type 316 stainless steel, J. Iron Steel Inst. 208 (1970) 1012–1014.
[4] K. Natesan, T.F. Kassner, Monitoring and measurement of carbon activity in sodium systems, Nucl. Technol. 19 (1973) 46–57, https://doi.org/10.13182/NT73-A31317.
[5] K.D. Ralston, N. Birbilis, The effect of grain size on corrosion: a review, MRS Proc. (2010) 1–13, https://doi.org/10.1557/proc-362-199.
[6] S.X. Li, Y.N. He, S.R. Yu, P.Y. Zhang, Evaluation of the effect of grain size on chromium carbide precipitation and intergranular corrosion of 316L stainless steel, Corros. Sci. 66 (2013) 211–216, https://doi.org/10.1016/j.corsci.2012.09.022.
[7] X. Yu, S. Chen, L. Wang, Effect of solution treatment conditions on the sensitization of austenitic stainless steel, J. Serbian Chem. Soc. 74 (2009) 1293–1302, https://doi.org/10.2298/JSC0911293Y.
[8] E.A. Trillo, R. Beltran, J.G. Maldonado, R.J. Romero, L.E. Murr, W.W. Fisher, A.H. Advani, Combined effects of deformation (strain and strain state), grain size, and carbon content on carbide precipitation and corrosion sensitization in 304 stainless steel, Mater. Charact. 35 (1995) 99–112, https://doi.org/10.1016/1044-5803(95)00072-0.
[9] H. Sahlaoui, K. Makhlouf, H. Sidhom, J. Philibert, Effects of ageing conditions on the precipitates evolution, chromium depletion and intergranular corrosion susceptibility of AISI 316L: experimental and modeling results, Mater. Sci. Eng. A 372 (2004) 98–108, https://doi.org/10.1016/j.msea.2003.12.017.
[10] E.A. Trillo, L.E. Murr, Effects of Carbon Content, Deformation, and Interfacial Energetics on Carbide Precipitation and Corrosion Sensitization in 304 Stainless Steel 47 (1999), pp. 235–245, https://doi.org/10.1016/S1359-6454(98)00322-X.
[11] H.E. Bühler, L. Gerlach, O. Greven, W. Bleck, The electrochemical reactivation test (ERT) to detect the susceptibility to intergranular corrosion, Corros. Sci. 45 (2003) 2325–2336, https://doi.org/10.1016/S0010-938X(03)00062-3.
[12] H. Shaikh, N. Sivaibharasi, B. Sasi, T. Anita, R. Amirthalingam, B.P.C. Rao, T. Jayakumar, H.S. Khatak, B. Raj, Use of eddy current testing method in detection and evaluation of sensitisation and intergranular corrosion in austenitic stainless steels, Corros. Sci. 48 (2006) 1462–1482, https://doi.org/10.1016/j.corsci.2005.05.017.
[13] C. Garcia, M.P. de Tiedra, Y. Blanco, O. Martin, F. Martin, Intergranular corrosion of welded joints of austenitic stainless steels studied by using an electrochemical minicell, Corros. Sci. 50 (2008) 2390–2397, https://doi.org/10.1016/j.corsci.2008.06.016.
[14] M.G. Pujar, N. Parvathavarthini, R.K. Dayal, S. Thirunavukkarasu, Assessment of intergranular corrosion (IGC) in 316(N) stainless steel using electrochemical noise (EN) technique, Corros. Sci. 51 (2009) 1707–1713, https://doi.org/10.1016/j.corsci.2009.04.028.
[15] V. Cihal, Intergranular Corrosion of Cr–Ni Stainless Steel, Unieux Conf., 1969.
[16] R.L. Fullman, A thermodynamic model of the effects of composition on the susceptibility of austenitic stainless steels to intergranular stress corrosion cracking, Acta Metall. 30 (1982) 1407–1415, https://doi.org/10.1016/0001-6160(82)90161-4.
[17] S.M. Bruemmer, Composition-based correlations to predict sensitization resistance of austenitic stainless steel, Corrosion 42 (1986) 27–35, https://doi.org/10.5006/1.3585149.
[18] N. Parvathavarthini, R.K. Dayal, Influence of chemical composition, prior deformation and prolonged thermal aging on the sensitization characteristics of austenitic stainless steels, J. Nucl. Phys. Mater. Sci. Radiat. Appl. 305 (2002) 209–219, https://doi.org/10.1016/S0022-3115(02)00915-7.
[19] C. Stawstrom, M. Hillert, An improved depleted-zone theory of intergranular corrosion of 18-8 stainless steel, J. Iron. Steel. Int. 207 (1969) 77–85.
[20] E.L. Hall, C.L. Briant, Chromium depletion in the vicinity of carbides in sensitized austenitic stainless steels, Metall. Trans. A, Phys. Metall. Mater. Sci. 15 A (1984) 793–811, https://doi.org/10.1007/BF02644554.
[21] G.S. Was, R.M. Kruger, A thermodynamic and kinetic basis for understanding chromium depletion in Ni-Cr-Fe alloys, Acta Metall. 33 (1985) 841–854, https://doi.org/10.1016/0001-6160(85)90108-7.
[22] H. Sahlaoui, H. Sidhom, J. Philibert, Prediction of chromium depleted-zone evolution during aging of Ni-Cr-Fe alloys, Acta Mater. 50 (2002) 1383–1392, https://doi.org/10.1016/S1359-6454(01)00444-X.
[23] T. Sourmail, C.H. Too, H.K.D.H. Bhadeshia, Sensitisation and Evolution of Chromium-Depleted Zones in Fe – Cr – Ni – C Systems 43 (2003), pp. 1814–1820.
[24] S. Kolli, T. Ohligschläger, D. Porter, Quantitative prediction of sensitization in austenitic stainless steel accounting for multicomponent thermodynamic and mass balance effects, ISIJ Int. 59 (2019) 1330–1336, https://doi.org/10.2355/isijinternational.isijint-2018-715.
[25] S. Kolli, T. Ohligschläger, J. Kömi, D. Porter, Sensitization and self-healing in austenitic stainless steel: quantitative prediction considering carbide nucleation and growth, ISIJ Int. (2019), https://doi.org/10.2355/isijinternational.isijint-2019-264.
[26] EN ISO 12732:2008: E, Corrosion of Metals and Alloys - Electrochemical Potentiokinetic Reactivation Measurement Using the Double Loop Method (based on Cihal's Method) (ISO 12732:2006), Finnish Stand. Assoc. SFS., 2008, p. 14.
[27] A.P. Majidi, M.A. Streicher, Double loop reactivation method for detecting sensitization in Aisi 304 Stainless Steels, Corrosion 40 (1984) 584–593, https://doi.org/10.5006/1.3581921.
[28] S. Rahimi, D.L. Engelberg, T.J. Marrow, Characterisation of grain boundary cluster compactness in austenitic stainless steel, Mater. Sci. Technol. 26 (2010) 670–675, https://doi.org/10.1179/026708309X12506933873783.
[29] S. Kolli, V. Javaheri, J. Kömi, D. Porter, On the role of grain size and carbon content on the sensitization and desensitization behavior of 301 austenitic stainless steel, Metals (Basel) 9 (2019), https://doi.org/10.3390/met9111193.
[30] Q. Chen, K. Wu, G. Sterner, P. Mason, Modeling precipitation kinetics during heat treatment with calphad-based tools, J. Mater. Eng. Perform. 23 (2014) 4193–4196, https://doi.org/10.1007/s11665-014-1255-6.
[31] J.S. Langer, A.J. Schwartz, Kinetics of nucleation in near-critical fluids, Phys. Rev. A 21 (1980) 948–958, https://doi.org/10.1103/PhysRevA.21.948.
[32] R. Kampmann, R. Wagner, P. Haasen, V. Gerold, R. Wagner, M.F. Ashby (Eds.), Kinetics of Precipitation in Metastable Binary Alloys—Theory and Application, Decomposition of Alloys: The Early Stages, 1984.
[33] Z. Hou, P. Hedström, Q. Chen, Y. Xu, D. Wu, J. Odqvist, Quantitative modeling and experimental verification of carbide precipitation in a martensitic Fe-0.16 wt%C-4.0 wt%Cr alloy, Calphad Comput. Coupling Phase Diagrams Thermochem. 53 (2016), pp. 39–48, https://doi.org/10.1016/j.calphad.2016.03.001.
[34] O. Prat, J. Garcia, D. Rojas, C. Carrasco, A.R. Kaysser-Pyzalla, Investigations on coarsening of MX and M23C6 precipitates in 12% Cr creep resistant steels assisted by computational thermodynamics, Mater. Sci. Eng. A 527 (2010) 5976–5983,

https://doi.org/10.1016/j.msea.2010.05.084.
[35] W. Xu, D. San Martin, P.E.J. Rivera Díaz del Castillo, S. van der Zwaag, Modelling and characterization of chi-phase grain boundary precipitation during aging of Fe-Cr-Ni-Mo stainless steel, Mater. Sci. Eng. A 467 (2007) 24–32, https://doi.org/10.1016/j.msea.2007.02.071.
[36] K. Frisk, Solubility of N in Cr-Fe-Mo-Ni alloys, Metall. Trans. A 23 (1992) 1271–1278, https://doi.org/10.1007/BF02665058.
[37] Caian Qui (Central South Univ. of Technology, Changsha, Thermodynamic analysis and evaluation of the Fe-Cr-Mn-N system, Metall. Trans. A (Physical Metall. Mater. Sci. (United States) 24 (11) (1993) 2393–2409, https://doi.org/10.1007/BF02646519.
[38] D. Kashchiev, Nucleation Basic Theory with Applications, Elsevier, 2000.
[39] P. Taylor, J. Feder, K.C. Russell, J. Lothe, G.M. Pound, Advances in Physics Homogeneous Nucleation and Growth of Droplets in Vapours, n.d.
[40] T.S. Ab, Thermo-Calc, (2008).
[41] A. Borgenstam, L. Höglund, J. Ågren, A. Engström, DICTRA, a tool for simulation of diffusional transformations in alloys, J. Phase Equilibria Diffus. 21 (2000) 269–280, https://doi.org/10.1361/105497100770340057.
[42] M. Lewis, B. Hattersley, Precipitation of M23C6 in austenitic steels, Acta Metall. 13 (1965) 1159–1168, https://doi.org/10.1016/0001-6160(65)90053-2.
[43] R.C. Pond, Review of the principal contrast effects observed at interphase boundaries using transmission electron microscopy, J. Microsc. 135 (1984) 213–240, https://doi.org/10.1111/j.1365-2818.1984.tb02530.x.
[44] M. Engineering, E. Paso, A TEM Investigation of M 23 C 6 Carbide Precipitation Behaviour on Varying Grain Boundary Misorientations in 304 Stainless Steels, 3 (n. d.) 1263–1271.
[45] Y. Yin, R.G. Faulkner, P. Moreton, I. Armson, P. Coyle, Grain boundary chromium depletion in austenitic alloys, J. Mater. Sci. 45 (2010) 5872–5882, https://doi.org/10.1007/s10853-010-4666-2.
[46] E.A. Trillo, L.E. Murr, A TEM investigation of M23C6 carbide precipitation behaviour on varying grain boundary misorientations in 304 stainless steels, J. Mater. Sci. 33 (1998) 1263–1271, https://doi.org/10.1023/A:1004390029071.